# Experimental and Simulation Studies of Partial Demagnetization Process of Permanent Magnets in Electric Motors

Mariusz Baranski, Wojciech Szelag, and Wieslaw Lyskawinski

***Abstract*—For the analysis of the process of partial demagnetization of permanent magnets (PMs) in electric machines, a field model of coupled electromagnetic and thermal phenomena was proposed. In the proposed approach the non-linearity of the magnetic circuit, the effect of temperature on the magnetic, electrical and thermal properties of the materials as well as the developed method for modeling the process of partial demagnetization of the PMs were taken into account. In order to verify the usefulness and effectiveness of the developed algorithm as well as software for analyzing the impact of temperature and the process of partial demagnetization of the magnets on the operation of a PM motor, the results of calculations were compared with the results of experimental studies. The experimental tests were carried out on a specially designed and constructed measuring test stand. The results of the research on the process of partial demagnetization of magnets in the line start permanent magnet synchronous motor (LSPMSM) are presented and the conclusions resulting therefrom have been formulated.**

***Index Terms*—Permanent magnet motors, partial demagnetization of permanent magnets, coupled electromagnetic-thermal phenomena, finite element analysis, influence of temperature on LSPMSM operation.**

## I. Introduction

An important disadvantage of electric machines excited by permanent magnets is the possibility of deterioration of their operational parameters by irreversible reduction of the main magnetic flux [1]. The value of this magnetic flux has an impact, among others on the electromagnetic torque generated in the machine, the electromotive force induced in the machine windings and efficiency of the machine [2]–[5]. This irreversible reduction of the magnetic flux may be caused by partial demagnetization of the permanent magnets. There are two main factors that can lead to the partial demagnetization of the magnets. These are the magnetic field generated by the armature winding and temperature [2], [6]–[10]. The source of the armature field are currents in the windings during machine operation. Particularly high values of the currents can occur in dynamic states of the machine. Such conditions include various types of short-circuits, start-up, reversal, and reconnection of the motor to the network immediately after the rotor falls out of synchronism [4]. In such operating states, currents with amplitudes even several times higher than the amplitude of the rated motor current may flow in the armature winding. The impact of the inrush magnetomotive force caused by the armature reaction may lead to partial demagnetization of the permanent magnets.

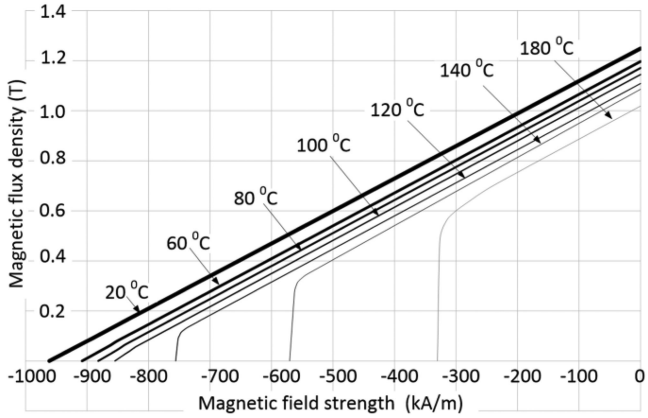


Fig. 1. Family of demagnetization characteristics $B(H,\tau)$ of magnetically hard N38SH material [9].

The susceptibility of magnets to partial demagnetization increases at higher temperatures. The effect of temperature on the magnetic properties of magnets is most often represented by a family of demagnetization characteristics [9], [10]. An example family of demagnetization characteristics of the N38SH grade magnet is shown in Fig. 1. The temperature of magnets in the motor depends on the power losses dissipated in the machine, the ability to transfer heat from the machine to the environment as well as the ambient temperature. Several heat sources can be identified in electrical motors. They cause power losses dissipated in windings, in magnetic circuits and in bearings [2], [13]–[16]. The sources of power losses are also eddy currents induced in solid conductive elements, e.g., permanent magnets. The largest power losses in the electric and magnetic circuits of the machine arise during the above discussed dynamic states of the motor operation. The temperature of the machine components is affected by both the duration and frequency of these conditions. In addition, this temperature depends on the amplitude of the currents in the windings, as well as the ambient

Manuscript received September 16, 2020; revised January 25, 2021 and April 7, 2021; accepted May 15, 2021. Date of publication May 31, 2021; date of current version November 23, 2021. This work was funded by Polish Government under Grant 0212/SBAD/0538. Paper no. TEC-00935-2020. *(Corresponding author: M. Baranski.)*

The authors are with the Faculty of Control, Robotics and Electrical Engineering, Poznan University of Technology, 60-965 Poznan, Poland (e-mail: mariusz.baranski@put.poznan.pl; wojciech.szelag@put.poznan.pl; wieslaw.lyskawinski@put.poznan.pl).

Digital Object Identifier 10.1109/TEC.2021.3082903

temperature. The accumulation of adverse thermal exposures can cause a large increase in the temperature of magnets and, as a consequence, lead to their partial demagnetization by the impact of armature magnetomotive force.

It should be emphasized that the process of partial demagnetization of the magnets is irreversible and causes permanent deterioration of functional parameters of the motor [2]–[4], [17]. For the above reasons, the research on problematic aspects of the process of partial demagnetization of PMs in permanent magnet machines is in the focus of many studies conducted over the last years [2], [18]–[20]. The research on the comprehensive analysis of the process of partial demagnetization of the magnets and minimization of its impact on functional parameters of motors are carried out in many scientific centers around the world [2], [4], [6]–[8], [18].

## II. State of the Art in Analysis of Partial Demagnetization of PM Machines

Based on the literature review, two main research directions related to the process of partial demagnetization of magnets in PM machines can be distinguished. The first direction concerns the analysis of the partial demagnetization process of PMs in machines using either analytical or more advanced numerical methods. While the second one is related to experimental research on the behavior of PMs subjected to external demagnetization and the impact of temperature on the magnetic properties of the magnets [6], [21], [22].

Focusing on the first direction the conducted over past decades research mainly tends to formulate accurate models and develops effective methods allowing one to predict the risk of partial demagnetization and its impact on PM machine's performance. Models of phenomena of different complexity are proposed for the analysis of the irreversible demagnetization process. Most of the models described in the literature are based just on the magnetization characteristic of magnets [6], [23], [24], however in papers [6], [7] the influence of temperature on the magnetic behavior in the external magnetic field is additionally taken into account. In the most complex approaches, models of the magnetic hysteresis phenomenon are used to map the partial demagnetization of magnets [11], [25], [26]. In the studies on the partial demagnetization process of PMs, to determine the magnetic fields which cause irreversible demagnetization of the magnets in electric machines the approaches based on simplified equivalent circuits [18], [22] as well as the finite element method [23], [24], [27], are used. In [1], [28], a combination of numerical integration of machine equations and the finite element method is used to study the irreversible demagnetization process. The discussed approaches were used to analyze the process of partial demagnetization of the magnets occurring, among others, during the start-up of an LSPMSM [27], [29], short circuits in the motor's electrical circuits [5], [30], motor falling out of synchronism [4], [5], [28] as well as in seeking design solutions allowing one to limit the risk of the partial demagnetization of magnets [7], [27]. Studies described in the literature, mostly present analyses of the partial demagnetization process carried out for the temperature of magnets [6], [7], that is set in advance. In [8], a simplified, thermal equivalent circuit of a motor was used to determine the temperature of the machine's components.

It should be emphasized, however, that in such approaches, the influence of temperature changes in machine components during transient states, e.g., during the start-up of a motors, cannot be taken into account. In order to take this effect into account, equations describing electromagnetic and thermal phenomena in the machine should be solved at the same time. There are few studies in the literature regarding the field analysis of transient states of PM machines taking into account coupling of electromagnetic and thermal phenomena [31]–[33]. There are even fewer papers in which, apart from the coupling of electromagnetic and thermal phenomena, the process of dynamic partial demagnetization of permanent magnets is included in the studies of PM machines during their operation [2], [3]. The process of dynamic partial demagnetization is understood as rapid changes in the magnetization state of magnets (and thus the main magnetic flux) caused by the change in current in the windings during the transient operating states of the machine. Of course, fast changes in the main magnetic flux affect the further course of the transients, and thus the dynamics of the motor.

In addition, it should be noted that commercially available software packages for the analysis of electromagnetic and thermal phenomena using the FEM do not allow one to carry out such comprehensive analysis of dynamic operating states of the PM machines, i.e., the analysis taking into account the impact of temperature and the process of partial demagnetization on the electromagnetic phenomena. For the above reasons, and considering the possible risk of permanent reduction of the main magnetic flux during the dynamic operation of the motor, the authors have attempted to develop a comprehensive method of analyzing the process of partial demagnetization of the magnets taking into account the influence of temperature. The developed field model of coupled electromagnetic and thermal phenomena as well as the algorithm for solving its equations are presented in Section III of the paper.

## III. Mathematical Model of Coupled Phenomena

The mathematical model of transient coupled phenomena in a PM motor includes equations describing the distribution of the magnetic field, currents in the windings, temperature distribution and the equation of the dynamics of movable elements in the drive system. It has been assumed that in the electromagnetically active region of the motor, magnetic and thermal fields are two-dimensional [2], [3]. Based on the above, the distribution of the transient magnetic field can be described by a system of equations [13]

$$\mathrm{curl}\left(\nu\ \mathrm{curl}\boldsymbol{A}\right) = -\sigma\left(\mathrm{d}\boldsymbol{A}/\mathrm{d}t + \mathrm{grad}V\right) + \mathrm{curl}\boldsymbol{M} \tag{1}$$

$$\boldsymbol{U} = \boldsymbol{R}i + \boldsymbol{L}\frac{\mathrm{d}}{\mathrm{d}t}\mathbf{i} + \frac{\mathrm{d}\Phi}{\mathrm{d}t} \tag{2}$$

where $\nu$ is the magnetic reluctivity of the domain, $\boldsymbol{A}$ is the magnetic vector potential, $\boldsymbol{J}$ is the current density vector, $\sigma$ is the conductivity of the medium, $\boldsymbol{M}$ is the magnetization vector in the region with the PMs, $V$ is the electric scalar potential, $\boldsymbol{U}$ is the vector of supply voltages, $\boldsymbol{R}$ and $\boldsymbol{L}$ are represent the matrix

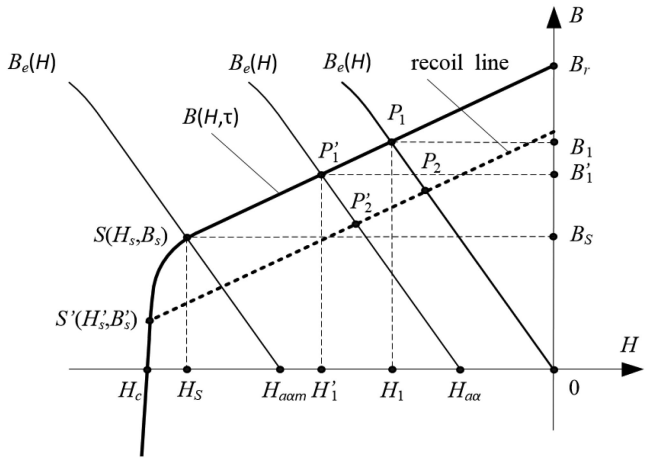


Fig. 2. Demagnetization characteristic $B(H,\tau)$ of the magnet - explanation of partial demagnetization process.

of loop resistances and the matrix of end-turn inductances, respectively, $\boldsymbol{i}$ is the vector of loop currents, $\Phi$ is the flux linkage vector calculated by means of the field model.

It has been assumed that the reluctivity $\nu = |\boldsymbol{H}|/|\boldsymbol{B}|$ of soft magnetic material is determined from the magnetic magnetization characteristics, while magnetization vector is determined by $\boldsymbol{M} = \nu_o \boldsymbol{B}$-$\boldsymbol{H}$ [2], where $\boldsymbol{B}$ is the vector of magnetic flux density, $\boldsymbol{H}$ is the magnetic field strength vector, $\nu_o$ is the reluctivity of the vacuum. When modeling the properties of magnetically hard material, it is assumed that it is characterized by rectangular magnetic anisotropy [34]. For each elemental volume of the magnet, a local coordinate system with orthogonal axes $\alpha$, $\beta$ is introduced and it is assumed that the $\alpha$ axis coincides with the direction of the magnetization vector $\boldsymbol{M}$. The use of local coordinate systems facilitates the description of magnetic properties of magnets and makes it possible to take into account the inhomogeneous distribution of the direction of magnetization in the magnet region. The magnetization of the magnet in the $\alpha$ direction depends on the intensity $H$ of the external magnetic field as well as on the magnet temperature and is calculated from the family of $B(H,\tau)$ demagnetization characteristics (see Fig. 1). In the case of the magnetization of the magnet in the $\beta$ direction it is assumed that the magnetization vector component is equal to zero.

To determine the magnetization from the $B(H,\tau)$ demagnetization characteristic, a model of partial demagnetization of the magnet has been proposed. It is based on the well-known behavior of magnetically hard material in the external magnetic field. In order to explain the functioning of the model, it has been assumed that the work point of the elemental volume of the magnet lies on the linear part of the demagnetization characteristic $B(H,\tau)$. In particular, with the absence of current in the armature winding, the operating point $P_1$ lies at the intersection of the $B(H,\tau)$ characteristic and the $B_e(H)$ characteristic of magnetization of the external magnetic circuit with respect to the considered elemental volume of the magnet (Fig. 2). During the machine operation, currents in the stator winding cause the armature magnetic field $H_a$. The $H_{a\alpha}$ component of the $\boldsymbol{H}_a$ field, acting in the direction of the $\alpha$ axis opposite to the magnetization vector $\boldsymbol{M}$, causes the work point $P_1$ to shift to the left on the $B(H,\tau)$ characteristic. As a result, the magnetic flux density is reduced from $B_1$ to $B_1$' and thus the magnetic flux produced by the permanent magnet decreases. When the armature field disappears, the flux density in the magnet returns to $B_1$. If the field amplitude $H_{a\alpha} > H_{a\alpha m}$ (where $H_{a\alpha} < 0$, $H_{a\alpha m} < 0$), then the work point will not move below the $S$ point and the armature field will not partially demagnetize the considered magnet volume (point $S$ is on the linear part of the characteristic $B(H,\tau)$). The irreversible, partial demagnetization of the magnet will occur if $H_{a\alpha} < H_{a\alpha m}$. Then the point $S$ will move along the bend on the demagnetization characteristic, e.g., to the point $S$', and the new magnet work point $P_2$ will then lie on the recoil line, marked as a dashed line in Fig. 2. Changing the position of the starting point $S$ of the recoil line on the demagnetization characteristic is called the magnet stabilization process. The presented process of the magnet stabilization is caused by the impact field of the armature. After the stabilization process, the flux density and field strength in the magnet depend on the location of the point $S$' on the $B(H,\tau)$ demagnetization characteristic and on the slope of the recoil line relative to the abscissa.

In order to model transient states of the PM motor, equations (1), (2) describing the magnetic field and currents in the electrical circuits, are solved together with the mechanical equilibrium equation of the drive system [2], [3]

$$J_i \frac{\mathrm{d}\omega}{\mathrm{d}t} = T_e - T_f - T_L \tag{3}$$

where $J_i$ is the moment of inertia of movable elements of the system, $\omega = \mathrm{d}\alpha/\mathrm{d}t$ is the angular velocity, $\alpha$ is the angular position of the rotor, $T_f$ is the friction torque, $T_L$ is the load torque, $T_e$ is the driving torque.

The power losses generated during motor operation in the windings, ferromagnetic core, solid conductive elements and bearings cause the increase temperature of the motor components. As the temperature changes, the electrical, magnetic and thermal properties of the materials the machine is made of also change [2], [3], [31]. Therefore, the proposed approach considers the equation describing thermal phenomena in the motor [2], [3]

$$\mathrm{div}\,(\lambda\,\mathrm{grad}\,\tau) + Q = c\rho\frac{\mathrm{d}\tau}{\mathrm{d}t} \tag{4}$$

where $\lambda$ is the tensor of thermal conductivity, $Q$ is the power loss density, $\tau$ is the temperature, $c$ is the specific heat and $\rho$ is the specific mass.

To model the boundary conditions for equation (4) it has been assumed that the heat flux $q_N$, passing through the domain boundary surface to the environment, is equal to the heat flux transferred to the environment by convection

$$q_N = h\frac{\partial\tau}{\partial N} = -\kappa\,(\tau_S - \tau_A) \tag{5}$$

where $N$ is the normal direction in relation to the domain boundary surface, $\tau_S$ is the temperature of boundary surface, $\tau_A$ is the ambient temperature, $\kappa$ is the heat transfer coefficient.

To solve equations (1)–(5) of the presented coupled model, numerical methods based on space and time discretization were used [2], [3], [13] and the authors applied the block –over relaxation method. It was assumed that the calculation blocks correspond to the particular equations of the used discrete model of coupled phenomena. An advantage of the block–over relaxation method is the possibility of using the classical effective Newton-Raphson procedure for an independent iterative solution of non-linear equations (1)–(5) [2]. The rotational movement of the rotor in discrete model of phenomena was implemented using the band method [35], while the electromagnetic torque $T_e$ in equation (3) was calculated on the basis of the magnetic field distribution determined by (1) [13], [35]. In order to reduce the calculation time, due to the lower dynamics of thermal phenomena in relation to electromechanical phenomena, the authors proposed the cascade approach of selecting the time-step length [36]. It consists in applying time steps of the same length in the analysis of an electromagnetic and thermal field during motor start-up, and then, after reaching an electromechanical steady-state, the length of the time step for thermal calculation is gradually increased. It should be emphasized that the advantage of the presented algorithm for the analysis of coupled electromagnetic and thermal phenomena is the possibility of taking into account the influence of temperature and the process of partial demagnetization of magnets on the transient states of the motor. The coupling between the transient electromagnetic, mechanical and thermal phenomena has not been included in commercially available software packages for analysis of machines excited by permanent magnets.

On the basis of the presented algorithm for solving the equations of the discrete model of coupled phenomena, the authors developed their own software to analysis the influence of temperature and inrush currents on the partial demagnetization of PMs in LSPMSMs.

## IV. Verification Studies of Developed Method of Coupled Phenomena Analysis

To verify the usefulness of the developed algorithm and software for the analysis of the coupled phenomena in LSPMSMs, the comparative analysis between the results of calculations and the results of experimental research has been carried out. The comparative analysis was carried out in two stages. First, the voltage induced in the stator winding of the machine at no-load was examined, and then the influence of the load torque on the starting process and the motor current was analyzed. In both stages of the experimental and simulation tests, the ambient temperature and the initial temperature of the motor components were inflicted.

Simulation and experimental tests have been conducted for the LSPMSM shown in Fig. 3. The excitation flux is produced by N38SH-type neodymium magnets arranged in a *U*-shape inside the rotor polar pitch area [2]. The stator phase winding is connected in a star configuration. The motor rated parameters have been summarized in Table I.

The experimental tests were carried out on a specially designed and built test stand – Fig. 4. The tested motor (1) was

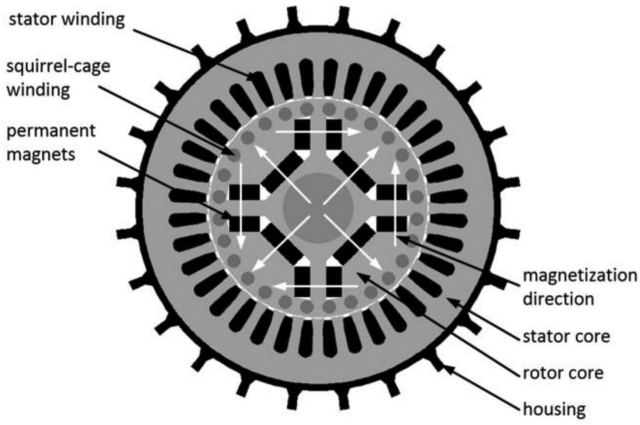


Fig. 3. The structure of LSPMSM motor.

TABLE I
Data of LSPMSM At 19.5Nm

| $U$ [V] | $I$ [A] | $f$ [A] | $\eta$ | cosφ |
|---|---|---|---|---|
| 400 | 5.4 | 50 | 0.89 | 0.93 |

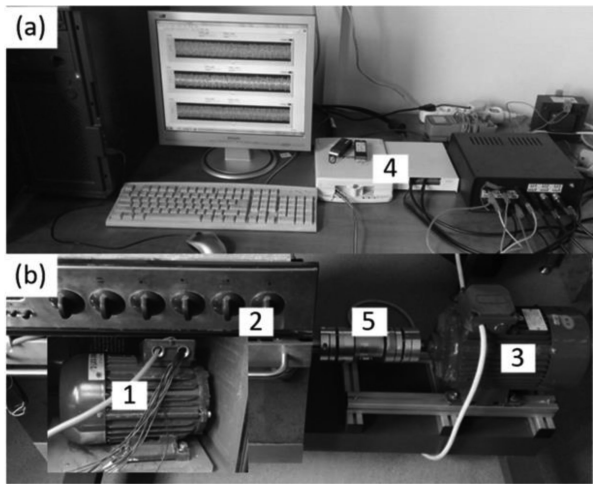


Fig. 4. General view of (a) measuring apparatus and (b) test stand, where 1 – LSPMSM motor, 2 – thermal chamber, 3 – driving motor/brake, 4 – data acquisition system, 5 – torque transducer.

placed in a thermal chamber (2) which enabled the temperature to be set from ambient to 250 °C.

Depending on the type of operation, the tested LSPMSM are coupled to the drive motor (3) (during generator operation of the machine) or to the magnetorheological brake (during motor operation). The advantage of the applied brake is the lack of torque pulsation. The temperature sensors of type PT-100 were used to measure the temperature of coils of different phase windings. These sensors are located along the circumference of the stator core, in the middle of the length of the slots, next to their openings near the winding surface. SCC-RTD01 modules for data acquisition from National Instruments Corporation (4) and an application developed in the LabVIEW environment were

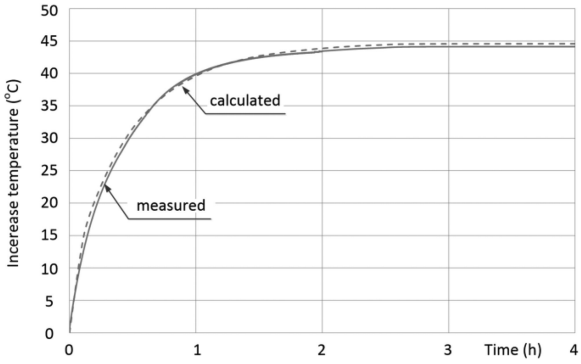


Fig. 5. Calculated and measured increase $\Delta\tau = \tau - \tau_A$ of the average temperature of the stator winding for $U = 400$ V and $T_L = 24$ Nm.

used to measure and record voltage, current, temperature and rotational speed [36] of the studied motor. A precise torque transducer of the MT100 type was used to measure torque on the motor shaft (5).

Before proceeding with the simulations of the partial demagnetization process, the developed discrete two-dimensional model of thermal phenomena had to be tuned in order to take into account the heat transfer in the plane toward the domain direction under consideration. The tuning process selected the value of the equivalent coefficient of the heat transferred from the motor to its ambience and described by the relationship (5) in such a way, in which the best compliance between the simulation results with the results of the experimental tests for the motor heating process was obtained. A comparison of the measured and calculated course of the average temperature increase in the area of the stator winding is shown in Fig. 5. The necessity to carry out the tuning process is caused, among others, by: a) the use of a two-dimensional model of thermal phenomena, b) strong dependence of the heat transfer coefficient on the speed of the cooling medium as well as the temperature and type of motor surface. Details of the tuning process of the applied thermal model are discussed in [36].

Next, the effect of motor temperature on the waveform and RMS value of the electromotive force $e(t)$ induced in the windings of the machine operating at no-load as a generator was analyzed. The tests were carried out for the thermally steady state at the rotation speed of the rotor equal to a synchronous speed of $n_s = 1500$ rpm.

The same machine operating conditions were reproduced in the simulation tests. It should be emphasized that the induced voltage tests were carried out immediately after installing magnetized permanent magnets in the motor. Thus, the magnets were not exposed to demagnetization before the machine tests, due to the high temperature and the impact magnetomotive force of the armature.

The measured and calculated line-to-line electromotive force (*emf*) $e_{\mathrm{L1\text{-}L2}}$ waveforms for given machine component temperatures equal to $\tau = 26$ °C and $\tau = 140$ °C, are shown in Fig. 6. Because the other line-to-line *emfs* differed only in their phase shift, their waveforms were not presented. The RMS values of the induced *emfs* are summarized in Table II. The table also gives the values of the coefficient determining the

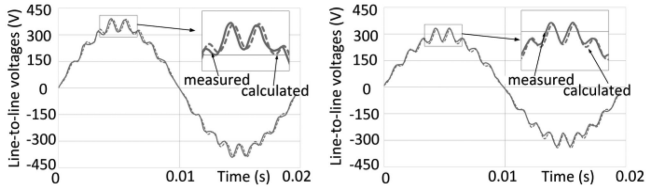


Fig. 6. Calculated and measured $e_{\mathrm{L1\text{-}L2}}(t)$ waveforms in $\tau = 26$ °C and $\tau = 140$ °C.

TABLE II
SUMMARY OF THE RMS OF THE BACK EMF AND BACK EMF COEFICIENT $\delta_{E\%}$

| $\tau$ [°C] | $E_C$ [V] | $E_M$ [V] | $\delta_{E\%}$ [%] |
|---|---|---|---|
| 26 | 323 | 332 | 2.56 |
| 60 | 313 | 324 | 3.49 |
| 100 | 303 | 314 | 3.60 |
| 140 | 291 | 298 | 3.80 |

discrepancy between the results of the calculations and measurements $\delta_{E\%} = ((E_M - E_C)/E_M)100\%$, where $E_M$ and $E_C$ are the RMS values of the voltages $e(t)$ obtained from the measurements and calculations, respectively. The table shows that the relative percentage difference between the results of the calculations and measurements is on a satisfactory level and does not exceed 3.80%.

The obtained results of the measurements and simulations confirm that the value of induced voltage decreases with increasing temperature. It can also be seen that the temperature due to nonlinearity of the ferromagnetic core has little effect on the shape of voltage waveforms.

In addition, based on a comparison of the effective values of the induced voltages $e(t)$ measured at the ambient temperature before as well as after the tests and carried out at temperatures up to 140 °C, it was found that the temperature did not affect the value of the induced voltage, and thus the main magnetic flux in the machine.

In order to further verify the developed algorithm for analyzing phenomena and the computer software as well as to examine the simultaneous effect of armature magnetomotive force (MMF) and temperature on the performance of the motor and magnetization state of the PMs, simulation and experimental tests of the starting process of the motor were carried out. Since the course of the LSPMSM start-up process depends on both the angular position of the rotor relative to the stator and the voltage phase at the instant of connecting the motor winding to the power grid [27], the simulation studies aimed to map identical operating conditions as on the test bench. For this reasons, it was assumed in a numerical model that for each simulation of the start-up process the motor was supplied with voltage of such a waveform and phase as were measured on the test bench. In addition, during the experimental test the rotor's angular position relative to the stator was set before each motor start-up. The start-ups were repeated for given values of the load moment $T_L$ and initial temperature $\tau_i = \tau$ ($t = 0$) of machine components.

In order to illustrate this stage of the research, Fig. 7 shows the waveform of one of the phase currents (in order to increase readability of the figure) and the rotational speed obtained during

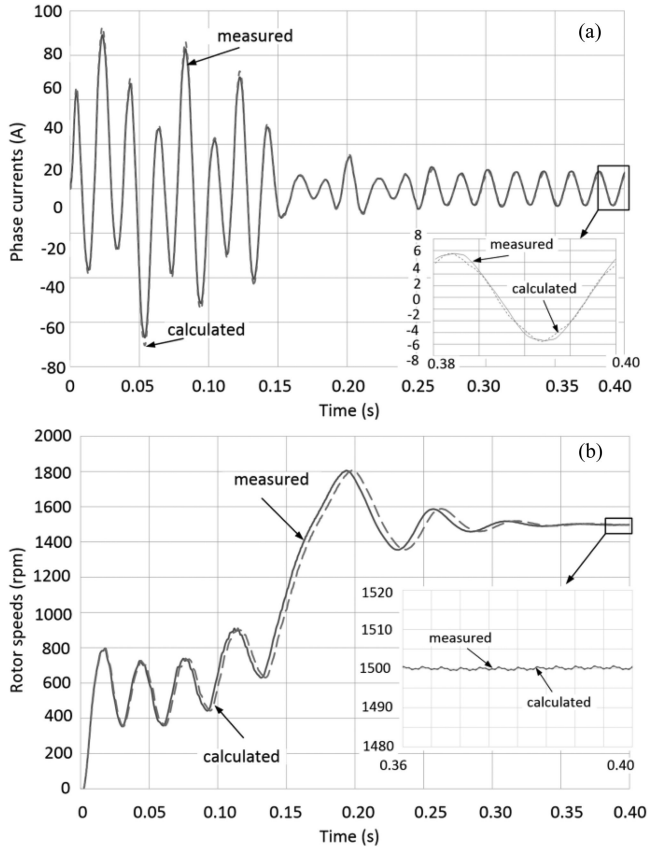


Fig. 7. Phase currents (a) and rotor speed (b) waveforms at $\tau_i = 100$ °C for $T_L = 19.5$ Nm, $J_i = 0.01$ kgm$^2$.

TABLE III
INFLUENCE OF TEMPERATURE AND LOAD TORQUE ON MOTOR CURRENT

| $\tau_i$ [°C] | $T_L$ [Nm] | $I_C$ [A] | $I_M$ [A] |
|---|---|---|---|
| 26 | 0 | 3.48 | 3.46 |
| 40 | | 3.59 | 3.57 |
| 60 | | 3.72 | 3.69 |
| 80 | | 3.89 | 3.85 |
| 100 | | 4.02 | 4.00 |
| | | | |
| 26 | 19.5 | 5.21 | 5.24 |
| 40 | | 5.33 | 5.36 |
| 60 | | 5.40 | 5.44 |
| 80 | | 5.48 | 5.50 |
| 100 | | 5.57 | 5.58 |

the motor's start-up performed for the load torque $T_L = 19.5$ Nm and initial temperature $\tau_i = 100$ °C. In addition, the figure shows a close-up of current and time waveforms for the last considered supply voltage period – representing the electromagnetic and electromechanical steady state operation conditions. The calculated $I_C$ and measured $I_M$ RMS values of phase current for the studied load torque and initial temperature of the motor have been summarized in Table III. The currents $I_C$ and $I_M$ have been calculated as well as measured at the electromechanical steady-state obtained immediately after the start-up of the motor.

Based on the comparison of the RMS value of the voltages $e(t)$ measured on the bench at the temperature $\tau_i = 26$ °C before and after the performed start-up tests, it was found that the temperatures $\tau_i$ up to 100 °C and inrush MMF of the armature at the start-up process did not cause a noticeable reduction in the induced voltage, and thus the demagnetization of the magnets. The performed comparative analysis between the simulation and experimental results shows that the developed algorithm and program for analyzing coupled phenomena maps the influence of temperature on the operation of LSPMSMs with a high degree of reliability.

In the authors' opinion, the differences between the results of the measurements and calculations are caused, among others, by: a) the assumption of a two-dimensional field in the machine, b) the accuracy of the measurements, c) discrepancies between the datasheet provided and real magnetic properties of the materials used, d) inaccuracies in the manufacturing process of components for magnetic circuits of the motor, e) errors of the applied method resulting from the assumed density of space and time discretization as well as the assumed accuracy of solving the equations of the discrete model. In order to minimize the effect of discretization on the obtained results, the length of the time step and density of the mesh were iteratively adjusted during the solving process. In the developed discrete 2D model of the LSPMS motor, the numbers of the calculated potentials $\varphi$ and temperatures $\tau$ of the mesh nodes were equal to approximately 37,000 and 40,000, respectively. Test calculations carried out on a PC with an Intel CORE i7 processor show that for a time step length of $\Delta t = 0.0001$s the calculation time for one supply voltage period was about 6 min.

## V. ANALYSIS OF PARTIAL DEMAGNETIZATION PROCESS

After completing the tests confirming the credibility of the obtained results, the modeling of temperature influence on the dynamic course of motor operation and the process of partial demagnetization of PMs have been carried out. The calculations were performed for the temperatures $\tau_i$ higher than 100 °C for which a high probability of partial demagnetization of the magnets occurs. It was also assumed that the magnets were fully magnetized at the beginning of simulations of the start-up process.

First, it was examined how the motor starting process affects the value and temperature distribution inside the machine immediately after the starting process, for $t = 0.6$ s. After this time, the electromechanical steady-state was obtained for each of the analyzed start-ups. Exemplary temperature distributions inside the PMs of the motor after the start-up process, for the time $t = 0.6$ s, are shown in Fig. 8. The initial temperature $\tau_i$ (equal to the ambient temperature $\tau_A$) and the highest temperature in the magnets can be read from the temperature scales located in the upper left corner of the figures. The performed tests showed that the highest temperature increase $\Delta\tau$ in the motor, of approximately 2.5 °C, was obtained at the start of the motor that drives the system characterized by a very high moment of inertia of the rotating masses ($J_i$ about 0.041 kgm$^2$) and negligibly low load torque. For this operating condition, the temperature rise in the magnets did not exceed 0.94 °C (Fig. 8a). The obtained temperature distributions show that the highest temperatures have magnet sub-areas near the rotor cage winding.

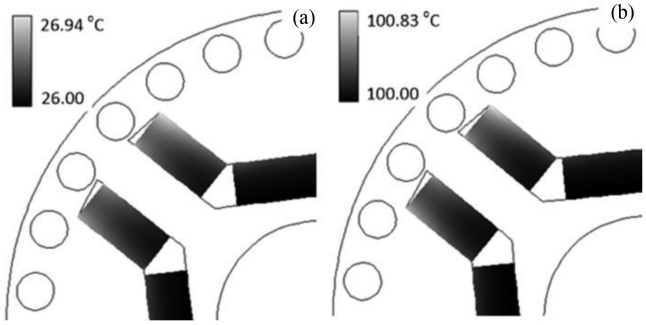


Fig. 8. Temperature distribution in magnets in an electromechanical steady-state after start-up for $t = 0.6$ s, $T_L = 0$ Nm, $J_i = 0.041$ kgm$^2$, a) $\tau_i = 26$ °C, b) $\tau_i = 100$ °C.

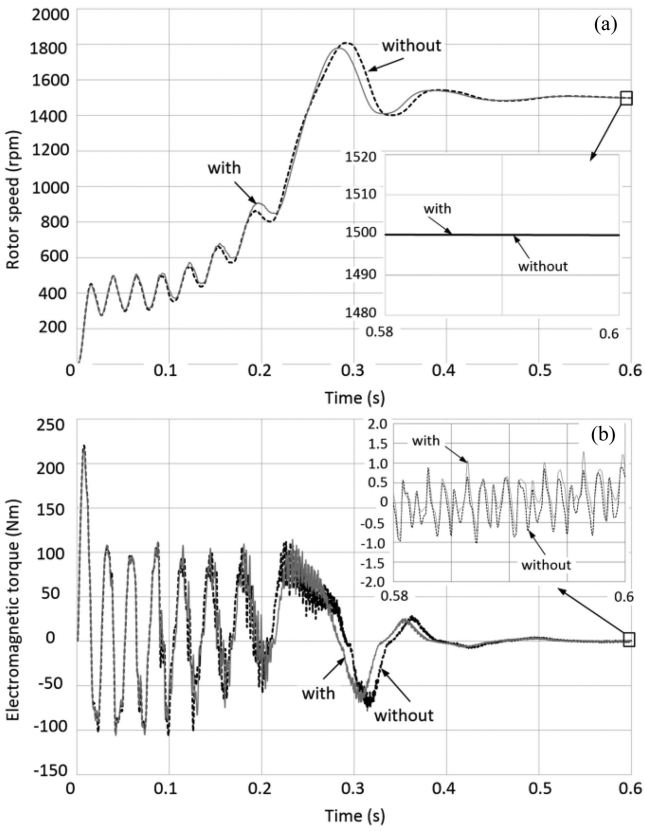


Fig. 9. Waveforms of (a) rotor speed $n(t)$ and (b) electromagnetic torque $T_e(t)$ during start-up at $T_L = 0.6$ Nm, $\tau_i = 26$ °C, $J_i = 0.041$ kgm$^2$ considering and neglecting the temperature impact.

The studies show that despite the observed slight increase in the temperature of the motor components, a change in the temperature of the windings and permanent magnets can clearly affect the start-up process. The impact of the temperature change during the start-up process has been illustrated in Fig. 9.

The waveforms of the speed $n(t)$ and torque $T_e(t)$, determined without taking into account the impact (without) and taking into account the effect (with) of temperature on the start-up process, have been compared.

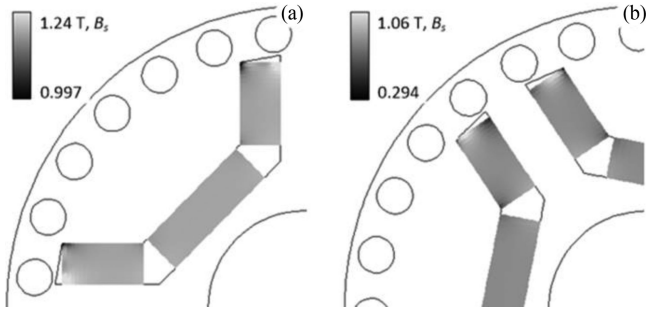


Fig. 10. Distribution of magnetic flux density $B_s$ a) before i b) after start- up process for $t = 0.6$s, $T_L = 19.5$ Nm, $\tau_i = 26$ °C, $J_i = 0.0082$ kgm$^2$.

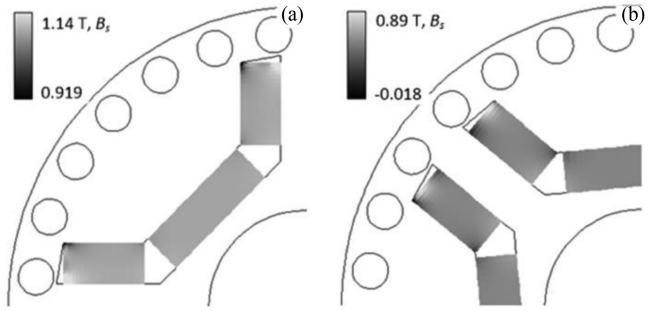


Fig. 11. Distribution of magnetic flux density $B_s$ a) before i b) after start-up process for $t = 0.6$ s, $T_L = 19.5$ Nm, $\tau_i = 100$ °C, $J_i = 0.01$ kgm$^2$.

In order to analyze the level of partial demagnetization of the permanent magnets, the location of the $S(H_s,B_s)$ point (see Fig. 2) on the $B(H,\tau)$ characteristic, describing the material properties, was studied. The comparisons of exemplary distributions of the magnetic flux density $B_s$ before and after starting the motor are shown in Figs 10 and 11. It follows that the magnetic flux density distributions $B_s$ before the start-up depend only on the temperature of the magnets. Whereas, the magnetic flux density distributions $B_s$ after the start-up depend additionally on the load torque and the moment of inertia of the rotating masses. It is observed that the magnetic flux density values $B_s$ can even be lower than zero. It should be emphasized, however, that the negative value of the magnetic flux density $B_s$ does not clearly determine partial demagnetization of the elemental sub-area. It has been assumed that partial demagnetization of the PM elemental sub-area takes place if the work point $S$ moves below the bend of the $B(H,\tau)$ characteristic – see Fig. 2. The selected results of the analysis of the impact of $\tau_i$ on the process of partial demagnetization of the magnets during the start-up of the LSPMSM are shown in Fig. 12. The magnet sub-areas where partial demagnetization of magnets took place are highlighted in dark gray. The figures show that the sub-areas located at the edges of the magnets are the most exposed to demagnetization.

The areas of partial demagnetization increase at higher temperatures $\tau$ of the magnets. A coefficient $\delta_{DE\%} = (E_B - E_A)/E_A \ 100\%$ was proposed to assess the degree of partial demagnetization of the magnets in the motor, where $E_B$ and $E_A$ are the RMS values of the voltage $e(t)$ determined for the same temperature of the machine components

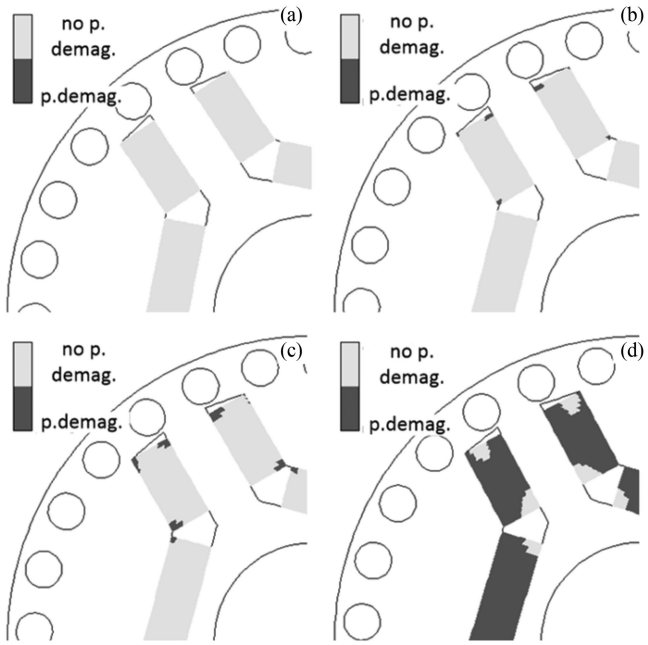


Fig. 12. Visualization of non-demagnetized (no p. demag.) and partially demagnetized (p. demag.) sub-areas of permanent magnets after start-up for $t = 0.6$s, $T_L = 19.5$Nm, $J_i = 0.041$ kgm$^2$ a) $\tau_i = 26$ °C, b) $\tau_i = 100$ °C, c) $\tau_i = 135$ °C, d) $\tau_i = 145$ °C.

TABLE IV
INFLUENCE OF TEMPERATURE ON THE DEGREE OF DEMAGNETIZATION $\delta_{\mathrm{DE}\%}$ OF PMS AFTER START-UP PROCESS FOR $T_1 = 19.5$ NM, $J_i = 0.0082$ KGM$^2$

| $\tau$ [°C] | 26 | 100 | 135 | 145 |
|---|---|---|---|---|
| $\delta_{DE\%}$ [%] | 0 | 0.003 | 0.210 | 12.723 |

before and after the process of partial demagnetization of the magnets. The values of the coefficient $\delta_{DE\%}$ obtained during the conducted studies are summarized in Table IV. The table shows that after the start-up carried out at a temperature of 145 °C, the electromotive force, and thus the main magnetic flux in the machine, decreased by over 12%. Such a large reduction in the magnetic flux at high temperatures results from the permanent magnet properties. The applied NdFeB magnets are characterized by significant decrease of immunity to the demagnetization with increase of the temperature. It is because the increase of temperature changes the shape of the demagnetization characteristic $B(H,\tau)$ and reduce the coercive field strength of the material – see Fig. 1. For example, the coercive field strength of the N38SH material at 145 °C decreases by approx. 40% in comparison to it coercive field strength at 20 °C.

## VI. CONCLUSION

The presented research shows that the proposed model as well as software developed by the authors are useful to study the impact of temperature on the process of partial demagnetization of magnets, considering electromechanical and electro-thermal transient states of the motor. The advantage of this model is a much higher reliability of the obtained results in relation to the models based on lumped parameters of the magnetic and thermal circuits of the motor, or on approaches in which the field equations describing electromagnetic phenomena and thermal phenomena are not solved simultaneously. The developed software makes it possible to evaluate whether the change in ambient temperature, voltage frequency and load torque will cause partial demagnetization of magnets and permanent deterioration of machine parameters. The proposed approach can also be used to optimize the structure of the motor in order to minimize the effect of inrush armature magnetic fields on PMs demagnetization. The research carried out was limited to the analysis of the machine in which the magnets were fully magnetized before the transient state occurred. When the motor was running in the propulsion systems, the PMs were repeatedly exposed to high temperatures and the impact of the armature MMF. The negative effects of these interactions can accumulate and gradually deteriorate the performance of the motor. Therefore, in further studies, it is expected that a new algorithm for the analysis of coupled phenomena will include the accumulation of multiple interactions that demagnetize magnets when a motor is in operation.

## REFERENCES

[1] G.-H. Kang, J. Hur, H. Nam, J.-P. Hong, and G.-T. Kim, "Analysis of irreversible magnet demagnetization in line-start motors based on the finite-element method," *IEEE Trans. Magn.*, vol. 39, no. 3, pp. 1488–1491, May 2003, doi: 10.1109/TMAG.2003.81033.
[2] M. Baranski, W. Szelag, and C. Jedryczka, "Influence of temperature on partial demagnetization of the permanent magnets during starting process of line start permanent magnet synchronous motor," *Intern. Symp. Elect. Mach. (SME)*, pp. 1–6, 2017, doi: 10.1109/ISEM.2017.7993535.
[3] M. Baranski, W. Szelag, and W. Lyskawinski, "An analysis of a start-up process in LSPMSMs with aluminum and copper rotor bars considering the coupling of electromagnetic and thermal phenomena," *Arch. Electr. Eng.*, vol. 68, no. 4, 2019, doi: 10.24425/aee.2019.130693.
[4] T. Zawilak, "Influence of rotor's cage resistance on demagnetization process in the line start permanent magnet synchronous motor," *Arch. Electr. Eng.*, vol. 69, no. 2, pp. 249–258, 2020, doi: 10.24425/aee.2020.133023.
[5] S. T. Lee, "Demagnetization study of an interior permanent magnet synchronous machine considering transient peak 3 phase short circuit current," in *2017 IEEE Energ. Conver. Cong. Expo. (ECCE)*, pp. 4694–4698, 2017, doi: 10.1109/ECCE.2017.8096800.
[6] S. Hamidizadeh, N. Alatawneh, R. R. Chromik, and D. A. Lowther, "Comparison of different demagnetization models of permanent magnet in machines for electric vehicle application," *IEEE Trans. Magn.*, vol. 52, no. 5, pp. 1–4, May 2016, doi: 10.1109/TMAG.2015.2513067.
[7] N. Nishiyama, H. Uemura, and Y. Honda, "Highly demagnetization performance IPMSM under hot environments," *IEEE Trans. Ind. Appl.*, vol. 55, no. 1, pp. 265–272, Jan. 2019, doi: 10.1109/TIA.2018.2863666.
[8] S. Ruoho, J. Kolehmainen, J. Ikaheimo, and A. Arkkio, "Interdependence of demagnetization, loading, and temperature rise in a permanent-magnet synchronous motor," *IEEE Trans. Magn.*, vol. 46, no. 3, pp. 949–953, 2010, doi: 10.1109/TMAG.2009.2033592.
[9] W. Yu *et al.*, "Coupled magnetic field-thermal network analysis of modular-spoke-type permanent-magnet machine for electric motorcycle," *IEEE Trans. Energy Conv.*, vol. 36, no. 1, pp. 120–130, Mar. 2021, doi: 10.1109/TEC.2020.3006098.
[10] P. Shahriari Nasab *et al.*, "Predicting temperature profile on the surface of a switched reluctance motor using a fast and accurate magneto-thermal model," *IEEE Trans. Energy Conv.*, vol. 35, no. 3, pp. 1394–1401, 2020, doi: 10.1109/TEC.2020.2974789.
[11] J. Chen *et al.*, "A hysteresis model based on linear curves for NdFeB permanent magnet considering temperature effects," *IEEE Trans. Magn.*, vol. 54, no. 3, pp. 1–5, Mar. 2018, doi: 10.1109/TMAG.2017.2763238.
[12] "[Online]. Available: https://www.arnoldmagnetics.com," Sep. 2020
[13] J. Driesen, "Coupled electromagnetic-thermal problems in electrical energy transducers," 2000.

[14] C. Huynh, L. Zheng, and D. Acharya, "Losses in high speed permanent magnet machines used in microturbine applications," *J. Eng. Gas Turbines Power*, vol. 131, no. 2, Mar. 2009, doi: 10.1115/1.2982151.
[15] Y. Wan, S. Cui, S. Wu, and L. Song, "Electromagnetic design and losses analysis of a high-speed permanent magnet synchronous motor with toroidal windings for pulsed alternator," *Energies*, vol. 11, no. 3, Art. no. 3, 2018, doi: 10.3390/en11030562.
[16] L. S. Maraaba, Z. M. Al-Hamouz, and M. A. Abido, "Mathematical modeling, simulation and experimental testing of interior-mount LSPMSM under stator inter-turn fault," *IEEE Trans. Energy Conv.*, vol. 34, no. 3, pp. 1213–1222, 2019, doi: 10.1109/TEC.2018.2886137.
[17] A. U. Ganesan and L. N. Chokkalingam, "Review on the evolution of technology advancements and applications of line-start synchronous machines," *IET Electric Power Appl.*, vol. 13, no. 1, pp. 1–16, 2019, doi: 10.1049/iet-epa.2018.5283.
[18] K.-C. Kim, K. Kim, H. J. Kim, and J. Lee, "Demagnetization analysis of permanent magnets according to rotor types of interior permanent magnet synchronous motor," *IEEE Trans. Magn.*, vol. 45, no. 6, pp. 2799–2802, 2009, doi: 10.1109/TMAG.2009.2018661.
[19] K.-C. Kim, S.-B. Lim, D.-H. Koo, and J. Lee, "The shape design of permanent magnet for permanent magnet synchronous motor considering partial demagnetization," *IEEE Trans. Magn.*, vol. 42, no. 10, pp. 3485–3487, 2006, doi: 10.1109/TMAG.2006.879077.
[20] P. Zhou, D. Lin, Y. Xiao, N. Lambert, and M. A. Rahman, "Temperature-Dependent demagnetization model of permanent magnets for finite element analysis," *IEEE Trans. Magn.*, vol. 48, no. 2, pp. 1031–1034, Feb. 2012, doi: 10.1109/TMAG.2011.2172395.
[21] S. Sjökvist and S. Eriksson, "Experimental verification of a simulation model for partial demagnetization of permanent magnets," *IEEE Trans. Magn.*, vol. 50, no. 12, pp. 1–5, Dec. 2014, Art no. 7401105, doi: 10.1109/TMAG.2014.2339795.
[22] H. Xiong, J. Zhang, M. W. Degner, C. Rong, F. Liang, and W. Li, "Permanent-Magnet demagnetization design and validation," *IEEE Trans. Ind. Appl.*, vol. 52, no. 4, pp. 2961–2970, Jul./Aug. 2016, doi: 10.1109/TIA.2016.2544739.
[23] S. S. Nair, V. I. Patel, and J. Wang, "Post-Demagnetization performance assessment for interior permanent magnet AC machines," *IEEE Trans. Magn.*,vol. 52, no. 4, pp. 1–10, Apr. 2016, Art no. 8102810, doi: 10.1109/TMAG.2015.2505245.
[24] W. N. Fu and S. L. Ho, "Dynamic demagnetization computation of permanent magnet motors using finite element method with normal magnetization curves," *IEEE Trans. Appl. Supercond.*, vol. 20, no. 3, pp. 851–855, Jun. 2010, doi: 10.1109/TASC.2009.2039787.
[25] M. Rosu, J. Saitz, and A. Arkkio, "Hysteresis model for finite-element analysis of permanent-magnet demagnetization in a large synchronous motor under a fault condition," *IEEE Trans. Magn.*, vol. 41, no. 6, pp. 2118–2123, Jun. 2005, doi: 10.1109/TMAG.2005.848319.
[26] G. Bavendiek *et al.*, "Magnetization dependent demagnetization characteristic of rare-earth permanent magnets," *Arch. Elect. Eng.*, vol. 68, no. 1, pp. 34–35, 2019, doi: 10.24425/aee.2019.125978.
[27] J.-X. Shen, P. Li, M.-J. Jin, and G. Yang, "Investigation and countermeasures for demagnetization in line start permanent magnet synchronous motors," *IEEE Trans. Magn.*, vol. 49, no. 7, pp. 4068–4071, 2013, doi: 10.1109/TMAG.2013.2244582.
[28] X. Y. Tang, X. Wang, G. Li, and M. Tian, "Demagnetization study of line-start permanent magnet synchronous motor under out-of-step and supersynchronous faults," *IEEE 11th Conf. Indus. Electr. Appl.(ICIEA)*, 2016, doi: 10.1109/ICIEA.2016.7603822.
[29] W. Lu, M. Liu, Y. Luo, and Y. Liu, "Influencing factors on the demagnetization of line-start permanent magnet synchronous motor during its starting process," in *2011 Internat. Conf. Elect. Mach. Syst.,*, pp. 1–4, 2011, doi: 10.1109/ICEMS.2011.6073886.
[30] S. Sjökvist and S. Eriksson, "Investigation of permanent magnet demagnetization in synchronous machines during multiple short-circuit fault conditions," *Energies*, vol. 10, no. 10, 2017, doi: 10.3390/en10101638.
[31] W. Jiang and T. M. Jahns, "Coupled electromagnetic–thermal analysis of electric machines including transient operation based on finite-element techniques," *IEEE Trans. Ind. Appl.*, vol. 51, no. 2, pp. 1880–1889, 2015, doi: 10.1109/TIA.2014.2345955.
[32] J.-B. Park, M. Moosavi, and H. A. Toliyat, "Electromagnetic-thermal coupled analysis method for interior PMSM,"*IEEE Int. Electric. Mach. Driv. Conf. (IEMDC)*, 2015, pp. 1209–1214, doi: 10.1109/IEMDC.2015.7409215.
[33] F. Marignetti, V. D. Colli, and Y. Coia, "Design of axial flux PM synchronous machines through 3-D coupled electromagnetic thermal and fluid-dynamical finite-element analysis," *IEEE Trans. Ind. Elect.*, vol. 55, no. 10, pp. 3591–3601, Oct. 2008, doi: 10.1109/TIE.2008.2005017.
[34] J. D. McFarland and T. M. Jahns, "Investigation of the rotor demagnetization characteristics of interior PM synchronous machines during fault conditions," *IEEE Energy Conv. Cong. Expo. (ECCE)*, pp. 4021–4028, 2012, doi: 10.1109/ECCE.2012.6342277.
[35] A. Demenko, "Movement simulation in finite element analysis of electric machine dynamics," *IEEE Trans. Magn* ., vol. 32, no. 3, pp. 1553–1556, May 1996, doi: 10.1109/20.497547.
[36] M. Baranski FE analysis of coupled electromagnetic-thermal phenomena in the squirrel cage motor working at high ambient temperature. *COMPEL - Int. J. Comput. Math. Elect. Electron. Eng.*, vol. 38, pp. 1120–1132, 2019, doi: 10.1108/COMPEL-10-2018-0384.

**M. Baranski** received the M.S. and Ph.D degrees in electrical engineering from the Poznan University of Technology, Poznan, Poland, in 2002 and 2010, respectively. He is currently with the Department of Mechatronics and Electrical Machines, Institute of Electrical Engineering and Electronics, Poznan University of Technology. His interests include finite-element simulation of static and dynamic electromagnetic and thermal phenomena in electric motors particular asynchronous and synchronous motors. Since 2010, he has been the Secretary of Editorial Board of Archives of Electrical Engineering.

**W. Szelag** received the M.S., Ph.D., and Doctor of Science degrees in electrical engineering from the Poznan University of Technology, Poznan, Poland, in 1979, 1984, and 1998, respectively. Since 1982, he has been employed in research and education. He is currently a Professor of electrical engineering with the Poznan University of Technology. He has authored or coauthored more than 200 conference and journal papers on electrical machines, electromagnetics, and electrodynamics. His research interests include electromagnetic field calculation, coupled electromagnetic-thermal and hydrodynamic phenomena analysis, and design of electrical machines and actuators.

**W. Lyskawinski** received the M.S. and Ph.D. degrees in electrical engineering from the Poznan University of Technology, Poznan, Poland, in 1990 and 1998, respectively. He is currently with the Department of Mechatronics and Electrical Machines, Institute of Electrical Engineering and Electronics, Poznan University of Technology. He deals with issues related to the analysis of operating states and the synthesis of pulse transformers and analysis of coupled electromagnetic, thermal and mechanical phenomena in electrical machines. His current research interests include design and analysis permanent magnet motors, and systems with magnetocaloric materials.